Inorganic Chemistry

Article

pubs.acs.org/IC

High-Pressure Raman Scattering of $CaWO_4$ Up to 46.3 GPa: Evidence of a New High-Pressure Phase

Pablo Botella,[†] Raúl Lacomba-Perales,[†] Daniel Errandonea,*[,†] Alain Polian,[‡,§] Placida Rodríguez-Hernández,[⊥] and Alfonso Muñoz[⊥]

[†]Departamento de Física Aplicada-ICMUV, Universidad de Valencia, MALTA Consolider Team, Edificio de Investigación, C. Dr. Moliner 50, 46100 Burjassot, Spain

[‡]IMPMC, Institut de Minéralogie, de Physique des Matériaux, et de CosmochimieSorbonne Universités, UPMC Univ Paris 06, 4 Place Jussieu, F-75005, Paris, France

[§]CNRS, UMR 7590, F-75005, Paris, France

[⊥]Departamento Física, Malta Consolider Team and Instituto de Materiales y Nanotecnología, Universidad de La Laguna, 38206 La Laguna, Tenerife, Spain

ABSTRACT: The high-pressure behavior of $CaWO_4$ was analyzed at room temperature by Raman spectroscopy. Pressure was generated using a diamond-anvil cell and Ne as pressure-transmitting medium. The pressure range of previous studies has been extended from 23.4 to 46.3 GPa. The experiments reveal the existence of two reversible phase transitions. The first one occurs from the tetragonal scheelite structure to the monoclinic fergusonite structure and is observed at 10 GPa. The onset of a previously unknown second transition is found at 33.4 GPa. The two high-pressure phases coexist up to 39.4 GPa. The Raman spectra measured for the low-pressure phase and the first high-pressure phase are consistent with previous studies in the pressure range where comparison is possible. The pressure dependence of all the Raman-active modes is reported for different phases. We also report total-energy and lattice-dynamics calculations, which determine the occurrence of two phase transitions in the pressure range covered by the experiments. The first transition is in full agreement with experiments (scheelite-to-fergusonite). According to calculations, the second-highest pressure phase has an orthorhombic structure (space group *Cmca*). Details of this structure, its Raman modes, and its electronic band structure are given. The reliability of the reported results is supported by the consistency between the theoretical and experimental values obtained for transition pressures, phonon frequencies, and phonon pressure coefficients.

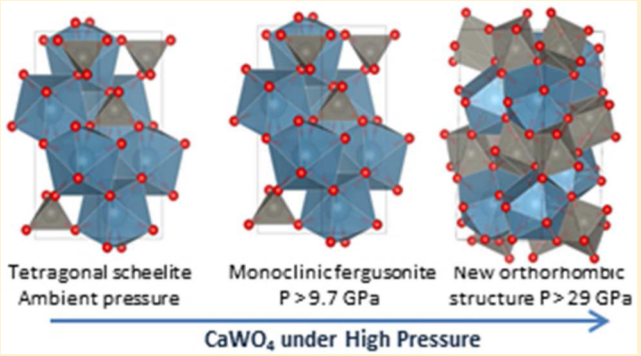

1. INTRODUCTION

$CaWO_4$, the mineral scheelite, crystallizes at ambient pressure and room temperature (RT) in a tetragonal structure with space group (SG) no. 88, $I4_1/a$, $Z = 4$. $CaWO_4$ is isomorphic with the alkaline-earth orthotungstates $SrWO_4$ and $BaWO_4$.[1] These compounds are technologically important materials and have a long history of practical applications, which include their use as solid-state scintillators,[2] laser-host materials,[3] detectors for X-rays and γ-rays in medical applications,[4] and in optoelectronic devices.[5] Additionally, several scheelite-structured and related zircon-structured oxides are found in Earth's crust. Therefore, the study of their high-pressure (HP) behavior has important geophysical implications.[6] In particular, scheelite is known to be the crystal structure of the HP phase of many zircon-type oxides, $CaWO_4$ being considered a prototype material for improving the understanding of the properties of ABO_4 oxides under extreme compression, which is an important focus of current work in condensed-matter science and inorganic chemistry.[6] When submitted to extreme pressure conditions, $CaWO_4$ and other orthotungstates exhibit several lattice instabilities, giving rise to a rich polymorphism.[6] As a consequence, they have been extensively studied under compression. However, further investigations are needed in order to define exactly the HP behavior of $CaWO_4$.

Raman spectroscopy is one of the most informative probes for studies of material properties under extreme conditions of HP.[7] This technique has been already used to study $CaWO_4$. The Raman spectrum of $CaWO_4$ at ambient conditions was first measured during the 1960s.[8] HP Raman studies were carried out at the beginning of the 1970s.[9] In this pioneer work, the existence of a pressure-induced transition at 1.5 GPa in $CaWO_4$ was reported. This study was carried out using NaCl as pressure-transmitting medium (PTM). Subsequent Raman

Received: May 30, 2014
Published: August 27, 2014

   dx.doi.org/10.1021/ic5012555 | *Inorg. Chem.* 2014, 53, 9729−9738

experiments extended the pressure range up to 4.2 GPa, using a 4:1 methanol–ethanol (ME) mixture as PTM, and found that the scheelite structure remained stable.[10] The pressure range of Raman experiments was extended up to 23.4 GPa by the end of the 20th century.[11] In this case, using ME as PTM a phase transition was found at 10 GPa. This transition has been confirmed by X-ray diffraction (XRD) and *ab initio* calculations.[12−14] The structure of the HP phase has been assigned to the monoclinic fergusonite structure (SG no. 15, $I2/a$, $Z = 4$). This structure is found to remain stable up to the highest pressure covered by XRD experiments (28 GPa),[14] but calculations predicted the occurrence of a second phase transition at 29 GPa.[13] Post-fergusonite phases have been found in related compounds,[15] but they have never been observed before in alkaline-earth orthotungstates. Another interesting fact on the HP behavior of these compounds is that transition pressures and structural properties can be influenced by the choice of the PTM used for the experiments.[14,16,17] All these facts evidence that more efforts are needed to accurately characterize the HP structural behavior of $CaWO_4$.

In this work, we report HP Raman measurements performed in $CaWO_4$ at RT using neon (Ne) as quasi-hydrostatic PTM. We extended the pressure range covered by Raman experiments from 23.4 GPa to 46.3 GPa. We found the existence of two reversible phase transitions. The scheelite–fergusonite transition is observed at 10 GPa, and the onset of a previously unknown transition at 34.4 GPa. We also carried out new *ab initio* calculations, which support the conclusions extracted from experiments, and propose a crystal structure for the second HP phase. Furthermore, we also theoretically studied the lattice vibrations and electronic properties of $CaWO_4$ under compression. The pressure evolution of all Raman modes of the scheelite, fergusonite, and new HP phases is reported. The results are discussed in comparison with previous investigations. They call for XRD and theoretical studies to determine the structure of the new HP phase found in this study.

2. EXPERIMENTAL METHODS

Samples used in the present experiments were obtained from a high-purity $CaWO_4$ single crystal that was grown with the Czochralski method starting from raw powders having 5N purity.[18] It was confirmed by XRD and Raman spectroscopy at ambient conditions that the crystal has only one phase with the scheelite structure. For the HP Raman experiment a 10 μm thick plate was cleaved from the crystal and loaded in a 300 μm culet diamond-anvil cell (DAC) together with a few ruby spheres of about 2 μm in diameter. The sample was loaded into a chamber 100 μm in diameter and 40 μm thick drilled in an Inconel gasket. Ne was used as PTM,[19] and pressure was determined by the ruby fluorescence technique.[20] The accuracy of the pressure determination was 0.1 GPa. Room-temperature Raman experiments were performed in the backscattering geometry using the 514.5 nm line of an Ar^+-ion laser. Recording spectra at different laser powers we found that an incident power of less than 100 mW before the DAC was appropriate for the present study. Under these conditions, the signal–noise ratio is optimized. Additionally, laser heating of the sample by the 514.5 nm laser is negligible in all the experiments we carried out because the laser energy is always below the band gap of $CaWO_4$ in the pressure range covered by the experiments.[21] A Mitutoyo 20× long working distance objective was employed for focusing the laser on the sample and for collecting the Raman spectra. The scattered light was analyzed with a Jobin-Yvon T64000 triple spectrometer equipped with a confocal microscope in combination with a low-background liquid-nitrogen-cooled multichannel charge-coupled device detector. In the experiments we used a 1200 grooves/mm grating and a 100 μm entrance slit. The wavenumber position was calibrated with reference to the first-order Raman line of a single crystal of silicon and Ar plasma lines. The spectral resolution in our measurements was better than 1 cm^{-1}.

3. OVERVIEW OF THE CALCULATIONS

The crystal structure and vibrational properties were simulated by means of *ab initio* total-energy calculations performed within the framework of the density functional theory (DFT).[22] The VASP[23] package has been used to carry out calculations with the pseudopotential method with a plane-wave expansion of the wave functions and the projector augmented wave scheme (PAW).[24] We employed PAW since it has more accurate pseudopotentials, which replace the core electrons and make smoothed pseudovalence wave functions; these pseudopotentials are different from those used in a previous study.[13] Highly converged results were achieved by extending the set of plane waves up to a kinetic energy cutoff of 520 eV. The exchange–correlation energy was taken in the generalized gradient approximation (GGA) with the Perdew–Burke–Ernzerhof (PBE[25]) prescription (we also used the PBE for solids, PBESOL,[26] and prescription, and we will report some results for comparison, but PBE was selected due to the systematic improvement of transition pressures). We also performed calculations using the exchange–correlation functional of Ceperley and Alder[27] (CA) parametrized by Perdew and Zunger[28] in the local density approximation (LDA). A dense Monkhorst–Pack[29] grid of k-special points was used to perform integrations along the Brillouin zone (BZ) in order to obtain very well converged energies and forces. At each selected volume, the structures were fully relaxed to their equilibrium configuration through the calculation of the forces on atoms and the stress tensor. In the final relaxed configurations at each specific volume (V) and pressure (P), the forces on the atoms are less than 0.003 eV/Å, and deviations of the stress tensor from a diagonal hydrostatic form are less than 0.1 GPa. It should be noted that the theoretical pressure, $P(V)$, can be obtained within the DFT formalism at the same time as the total energy, $E(V)$. The theoretical pressure, P, like other derivatives of the energy, is obtained from the calculated stress. From the theoretical point of view a phase transition between two structures occurs when at a given pressure the enthalpy ($H = E + PV$) is the same for both structures (all the simulations are at 0 K and do not include the zero-point contribution); this method has been well tested in many compounds related to $CaWO_4$.[30] We analyzed a limited number of structures and obtained clear candidates to explain the phase transition sequence, so we cannot excluded other possible unanalyzed structures.

Lattice-dynamics calculations were performed at the zone center (Γ point) of the BZ. Highly converged results on forces are required for the calculation of the dynamical matrix using the harmonic approximation in the direct force constant approach.[31] The construction of the dynamical matrix at the Γ point of the BZ involves separate calculations of the forces in which a fixed small displacement from the equilibrium configuration of the atoms within the primitive cell is considered. The number of such independent displacements for the different structures is reduced due to the crystal symmetry. Diagonalization of the dynamical matrix provides the frequencies of the normal modes. Moreover, these calculations allow identifying the symmetry and eigenvectors of the phonon modes in each structure at the Γ point. For completeness we also carried out band-structure calculations,

dx.doi.org/10.1021/ic5012555 | Inorg. Chem. 2014, 53, 9729−9738

which have been performed with VASP. Technical details of these calculations can be found in our previous works, where the methodology is extensively described.[32,33]

To close this section, we will make a comment on spin−orbit (SO) interaction. Due to the heavy mass of the W atoms, this interaction is not negligible for 5d transition metals such as W.[34] Therefore, we also performed, at selected pressures, calculations of the different physical properties of $CaWO_4$ including the SO coupling. This greatly increases the computational time required for the simulations. However, the obtained results considering the SO coupling do not appreciably differ from the results achieved without including SO effects. Thus, to systematically evaluate the effect of pressure on the different phases of $CaWO_4$, calculations were performed neglecting the SO interaction.

4. EXPERIMENTAL RESULTS

It is well known that group-theory considerations lead for the scheelite structure to 13 zone-center Raman-active modes: $\Gamma = 3A_g + 5B_g + 5E_g$.[8,11,35] In this structure each W is surrounded by four equivalent oxygen atoms forming an isolated tetrahedron. On the other hand, each Ca is surrounded by eight oxygen atoms forming a dodecahedron. As a consequence, the Raman modes have been classified either as internal (υ), when the WO_4 center of mass does not move, or as external, when they imply movement of the WO_4 tetrahedron as a rigid unit. The external (lattice) modes can be divided into those involving rotations (R) or translations (T).[36] Figure 1 shows a selection of Raman spectra collected in $CaWO_4$ up to 31.6 GPa. From ambient pressure to 9.7 GPa the 13 modes of the scheelite-type structure have been identified. As typical in scheelites, the most intense mode is the highest frequency mode associated with a symmetric stretching internal vibration of the WO_4 tetrahedron.[11] Table 1 summarizes the Raman frequencies (ω_0) at ambient pressure, which are compared with previous experiments.[8−11] The agreement with different studies is quite good. The mode assignment has been done following the literature[8,11,35] and our calculations.

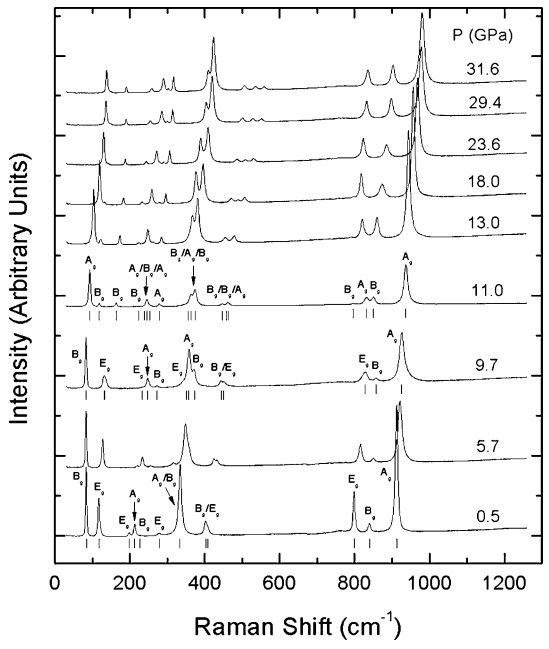

Figure 1. Selection of Raman spectra collected under compression up to 31.6 GPa. For $P \leq 9.7$ GPa they correspond to the scheelite phase and for $P \geq 11$ GPa to the fergusonite phase. Ticks identifying Raman modes are given together with the mode assignment at 0.5, 9.7, and 11 GPa.

From the experiments, we follow the pressure evolution of all the Raman modes of the scheelite-type $CaWO_4$, which is shown in Figure 2. The dependence of the phonon frequencies with pressure is nearly linear. The pressure coefficients ($\partial\omega/\partial P$) calculated assuming linear dependences are summarized in Table 1. The reported Grüneisen parameters, $\gamma = (B_0/\omega_0)(\partial\omega/\partial P)$, were calculated assuming for the bulk modulus an average of the values determined from quasi-hydrostatic experiments, $B_0 = 76$ GPa.[14] In the table, it can be seen that most modes harden under compression. The E_g mode at 274 cm^{-1} is the hardest one (see Figure 2). This mode is associated with a rotation lattice mode.[23] On the other hand, the internal A_g (332 cm^{-1}) and B_g modes (334 cm^{-1}), which are very close in frequency at ambient pressure, gradually split into two well-resolved peaks under compression. In particular, at 9.7 GPa their frequencies are 358 cm^{-1} (A_g) and 372 cm^{-1} (B_g). The reason for the different pressure coefficients of the two modes is that the A_g mode only implies the movement of O atoms, while the B_g mode introduces an additional displacement of Ca along the *c*-axis, and thus it should be more sensitive to pressure.[8] Another feature to highlight is that the lowest frequency mode (B_g at 85 cm^{-1}) is found to soften with pressure. This is a translation lattice mode.[23] The softening of this mode upon compression is a typical feature of scheelite-type oxides.[24,37] In Table 1, it can be seen that our quasi-hydrostatic experiments give slightly different pressure coefficients for the Raman modes than non-hydrostatic experiments.[9−11] When compared with experiments done using ME as PTM, differences are mainly within 10%, but with the experiment done under NaCl the differences are larger. The comparison with calculations will be done in the next section, where the good agreement between our experiments and the calculations will be shown.

When compressing $CaWO_4$ from 9.7 GPa to 11 GPa, several modifications on the Raman spectra take place. In particular, numerous extra modes appear, reaching a total of 18 Raman modes. The observed changes can be assigned to the occurrence of a phase transition in agreement with previous Raman[11] and XRD[12−14] experiments that reported the transition at a similar pressure. The structure of the HP phase has been undoubtedly assigned to the monoclinic fergusonite structure.[12−14] In contrast with previous experiments[11] no evidence of phase coexistence of the low- and high-pressure phases has been detected in our experiments. This is probably because radial pressure gradients are small in our experiments thanks to the use of Ne as PTM. According to group theory, the fergusonite structure has 18 Raman-active modes: $\Gamma = 8A_g + 10B_g$. This is in agreement with our observation. Previously only 15 modes of the 18 were reported.[11] In Table 2, we show the Raman-active phonons detected in the fergusonite phase and their pressure coefficients. Some modes happened to be difficult to identify because there were two modes very close in frequency (e.g., the A_g and B_g modes at 339 and 346 cm^{-1}; see Table 2). However, with the help of the present calculations, after doing a Lorentzian multipeak fitting analysis, we have been able to deconvolute the different modes and to determine the frequency of the 18 modes of fergusonite $CaWO_4$. Note that because of the pressure-induced mode merging (see Figure 2), some modes can be detected only up to 27.6 or 36 GPa, as indicated in Table 2. The mode assignment for fergusonite $CaWO_4$ has been done based upon our calculations, because we performed nonpolarized Raman measurements.

The pressure evolution of the Raman modes is shown in Figure 2. As reported by Christofilos et al.,[11] it can be seen in the figure that there is a change in the pressure behavior of some modes near 15.5 GPa. One clear example of this phenomenon is two of the high-frequency modes (B_g 796 cm^{-1} and Ag 833 cm^{-1}), which after the transition have a negative pressure coefficient up to 15.5 GPa, but beyond this pressure the phonon frequencies increase under compression. The change observed in the pressure coefficients $d\omega/dP$ is much larger than the uncertainty of this magnitude. The same nonlinear pressure dependence for some of the phonons of the HP phase has been observed in $SrWO_4$.[11] A similar unusual behavior has

dx.doi.org/10.1021/ic5012555 | Inorg. Chem. 2014, 53, 9729−9738

Table 1. Frequencies at Ambient Pressure (ω_0), Pressure Coefficients ($d\omega/dP$), and Grüneisen Parameters ($\gamma = (B_0/\omega_0)(\partial\omega/\partial P)$) for the Raman-Active Modes of Scheelite $CaWO_4$[a]

mode	ω_0,[b] cm^{-1}	$d\omega/dP$,[b] cm^{-1}/GPa	γ[b]	ω_0,[c] cm^{-1}	$d\omega/dP$,[c] cm^{-1}/GPa	ω_0,[d] cm^{-1}	$d\omega/dP$,[d] cm^{-1}/GPa	ω_0,[e] cm^{-1}	$d\omega/dP$,[e] cm^{-1}/GPa	ω_0,[f] cm^{-1}	ω_0,[g] cm^{-1}	$d\omega/dP$,[g] cm^{-1}/GPa	ω_0,[h] cm^{-1}	$d\omega/dP$,[h] cm^{-1}/GPa
$T(B_g)$	85	−0.1	−0.08	86	−1.1	84	−0.4	86	0	84	76	−0.8	83	−0.8
$T(E_g)$	117	1.7	1.10	117	1.4	116	1.7	117	0−3.9	117	115	1.8	110	1.9
$T(E_g)$	197	4.0	1.48	195	4.5	196	3.7	195	3.9	195	191	4.7	176	5.6
$T(A_g)$	210	4.0	1.45	210	3.9	212	3.8	210	4.3	210	210	4.1	197	4.1
$R(B_g)$	226	4.2	1.41			227	4.7	218	6.1	218	218	6.1	200	7.3
$R(E_g)$	274	7.7	2.14	273		276	7.0	275	8.6	275	274	7.5	251	7.2
$\upsilon_2(A_g)$	332	2.7	0.62	334	2.4	334	2.5	336	2.5	336	318	2.4	313	2.0
$\upsilon_2(B_g)$	334	4.1	0.93			334	2.5	336	4.9	336	322	4.2	312	4.3
$\upsilon_4(B_g)$	401	4.4	0.83	401	4.8	402	4.1	401	4.3	401	388	4.1	377	3.6
$\upsilon_4(E_g)$	404	4.6	0.86			406	4.6	409	4.0	409	393	4.9	380	4.8
$\upsilon_3(E_g)$	798	3.1	0.30	797	3.0	797	3.0	797	2.0−6.6	797	789	3.1	774	3.5
$\upsilon_3(B_g)$	839	1.9	0.17	838	1.6	838	1.9	838	0	838	823	1.9	812	2.4
$\upsilon_1(A_g)$	912	1.5	0.13	912	1.4	911	1.5	912	2.1	912	895	1.6	886	1.7

[a]To calculate γ, we used B_0 = 76 GPa.[14] Present experimental frequencies are given with an accuracy of 1 cm^{-1} and pressure coefficients with an accuracy of 0.1 cm^{-1}/GPa. [b]Present experimental results are compared with the literature. [c]Ref 10. [d]Ref 11. [e]Ref 9. [f]Ref 8. The results from the present theoretical calculations are also given for comparison. [g]PBESOL functional. [h]PBE functional.

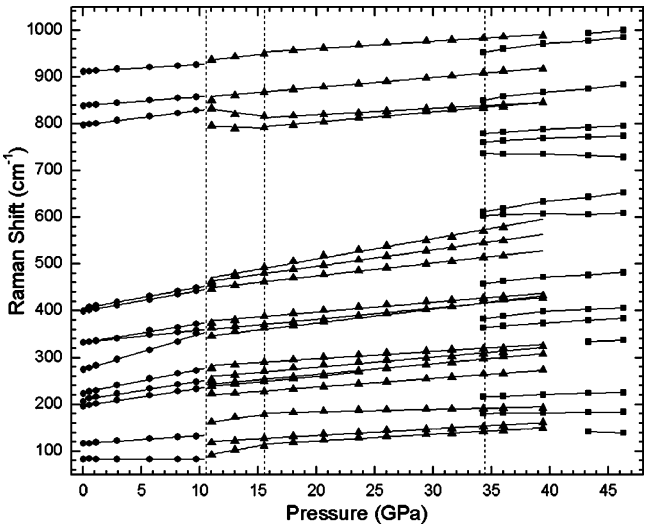

Figure 2. Pressure dependence of the Raman modes of the scheelite (circles), fergusonite (triangles), and new HP (squares) phases. For scheelite and fergusonite, solid lines represent a fit to the experimental data (see text); for the new phase they are a guide to the eye. All data points were obtained from spectra collected under compression. The vertical dashed lines indicate the scheelite−fergusonite transition pressure (left), the pressure where a slope change is found for some modes in fergusonite (center), and the onset pressure of the second phase transition (right).

been found in superconducting arsenates,[38] being identified with a lattice modification induced by pressure. In the case of $CaWO_4$, according to XRD experiments,[14] the unit-cell parameters of the fergusonite phase also have nonlinear pressure dependences. In particular, the *a*-axis increases with pressure from 10 to 15 GPa, reaching a maximum at this pressure and decreasing beyond 15 GPa.[14] This fact induces a reduction of the spontaneous strain of the monoclinic structure,[39] which should be reflected in the vibrational properties of fergusonite. In the following, we will use the correlation between the nonlinear behavior of the unit-cell parameters of $CaWO_4$ (and consequently of bond distances) and of some of the phonon frequencies to try to explain the nonlinear behavior of several of the Raman modes of the fergusonite phase. The WO_4 tetrahedron in scheelite is regular, but after the transition to fergusonite, it becomes nonregular, having two different W−O distances.[14] As a consequence, one of the modes assigned to an internal vibration of the WO_4 tetrahedron in scheelite splits into two modes of fergusonite. These are the B_g (796 cm^{-1}) and A_g (833 cm^{-1}) modes, which show a nonlinear behavior. They correspond basically to stretching vibrations associated with the short W−O distance. From the structural data reported in ref 14 and from our calculations, it can be seen that the structural changes induced by pressure in fergusonite cause a nonisotropic deformation of the WO_4 tetrahedron. Up to 15 GPa the tetrahedron deformation is accompanied by a small tilting of it. This causes a decrease with pressure of the long W−O distance and an increase of the short W−O distance (the total volume of the tetrahedron is reduced). We think that this bond increase can be the cause of the phonon softening observed up to 15.5 GPa. At pressures higher than 15 GPa, the tetrahedral tilting is negligible and the WO_4 is compressed in a nearly isotropic way. Then it is reasonable that both the B_g (796 cm^{-1}) and A_g (833 cm^{-1}) modes harden upon compression beyond 15.5 GPa. The same correlation can be made with the response to pressure of Ca−W distances and the low-frequency external modes that follow a nonlinear behavior. A deeper discussion about the origin of the unusual pressure behavior above-described for some phonons of fergusonite is beyond the scope of this work.

In Table 2 it can be seen that our frequencies determined for fergusonite at 11 GPa compare well with those of the 15 modes previously determined at 10.5 GPa.[11] In addition, we report the frequency of the three modes previously undetected for fergusonite $CaWO_4$. These modes are those we found at 118, 339, and 796 cm^{-1}. Regarding the pressure coefficients, only 10 of them were reported before.[11] Here, we report the 18 pressure coefficients. For the modes following a linear behavior, $\partial\omega/\partial P$ was determined from the whole pressure range where the modes can be detected (as indicated in Table 2). For the five modes that follow a nonlinear behavior we provide the pressure coefficient determined for P > 15.5 GPa, which was determined assuming linear pressure dependences for the phonons on the selected pressure range (see Table 2). For these five modes pressure coefficients have not been determined for P < 15.5 GPa because we have only three data points for this pressure range. The agreement of the pressure coefficients here and previously[11] determined is not as good as the agreement of the frequencies (see Table 2). In particular, we found large discrepancies for the A_g modes with a frequency 278 cm^{-1}. For this mode, our pressure coefficient is less than half of the value previously reported.[11] We attribute this discrepancy to the use of different PTM in the experiments. This hypothesis is supported by two facts: (1) It is well known that beyond 10 GPa Ne is much more quasi-hydrostatic than ME.[19] (2) It is known that deviatoric stresses influence the pressure behavior of the Raman vibrations in scheelite-type oxides.[16,17]

dx.doi.org/10.1021/ic5012555 | Inorg. Chem. 2014, 53, 9729−9738

Table 2. Frequencies and Pressure Coefficients for the Raman-Active Modes of Fergusonite $CaWO_4$[a]

mode	$\omega_{11\ GPa}$,[b] cm^{-1}	pressure range,[b] GPa	$d\omega/dP$,[b] cm^{-1}/GPa	$\omega_{10.5\ GPa}$,[c] cm^{-1}	$d\omega/dP$,[c] cm^{-1}/GPa	$\omega_{11.4\ GPa}$,[d] cm^{-1}	pressure range,[d] GPa	$d\omega/dP$,[d] cm^{-1}/GPa	$\omega_{12.4\ GPa}$,[e] cm^{-1}	pressure range,[e] GPa	$d\omega/dP$,[e] cm^{-1}/GPa
*A_g	92	15.5–39.4	1.5	90		112	9–21	3.5	95	18.5–29.4	1.2
B_g	118	11–39.4	1.4			123	9–21	3.1	114	10.7–29.4	1.5
*B_g	163	15.5–39.4	0.5	162		171	9–21	2.23	162	18.5–29.4	0.5
B_g	223	11–39.4	1.9	217	1.8	214	9–21	2.9	210	10.7–29.4	2.2
A_g	246	11–27.6	2.3	242	2.0	236	9–21	2.8	234	10.7–29.4	2.5
B_g	253	11–39.4	2.2	258	2.7	254	9–21	2.3	243	10.7–29.4	2.2
A_g	278	11–39.4	1.6	277	3.5	268	9–21	2.1	265	10.7–29.4	3.6
A_g	339	11–39.4	2.4			341	9–21	2.7	345	10.7–29.4	1.3
B_g	346	11–39.4	3.0	355	3.1	345	9–21	4.1	330	10.7–29.4	3.9
A_g	363	11–39.4	2.4	359		369	9–21	2.3	355	10.7–29.4	2.3
B_g	374	11–39.4	2.1	373	3.1	379	9–21	4.8	363	10.7–29.4	4.6
B_g	447	11–36	2.8	445	3.0	438	9–21	2.9	425	10.7–29.4	4.7
B_g	457	11–36	3.5	461	3.4	447	9–21	3.8	444	10.7–29.4	2.8
A_g	462	11–36	4.4	461		472	9–21	4.0	449	10.7–29.4	4.2
*B_g	796	15.5–39.4	2.2			761	9–21	2.3	765	18.5–29.4	2.4
*A_g	833	15.5–39.4	1.4	833		786	9–21	0.59	798	18.5–29.4	1.4
B_g	850	11–39.4	2.9	848	3.9	844	9–21	3.2	832	10.7–29.4	3.6
*A_g	937	11–39.4	3.0	935	2.9	924	9–21	3.4	912	10.7–29.4	3.2

[a]Present experimental frequencies are given with an accuracy of 1 cm^{-1} and pressure coefficients with an accuracy of 0.1 cm^{-1}/GPa. The pressures at which the frequencies are determined are indicated. In those modes in which a nonlinear behavior is found we provide pressure coefficients for a pressures range where a nearly linear behavior can be assumed. The pressure range is indicated. The nonlinear modes are denoted with an asterisk. [b]Present experimental results are compared with the literature. [c]Ref 11 and present calculations. [d]PBESOL. [e]PBE.

We will qualitatively comment now on the classification of the Raman modes of the fergusonite phase of $CaWO_4$. The structural similarity between scheelite and fergusonite allows identifying the Raman modes of the second structure also as internal and external modes.[35] It is known that in fergusonite the tetrahedral coordination of W is retained,[12−14] with only a slight distortion of the WO_4 tetrahedron. Therefore, drastic changes are not expected in the frequencies of the internal modes. This can be seen in Figures 1 and 2. In particular, the main change in the internal modes at the transition is the splitting of the E_g modes of scheelite (which are double degenerate). Note that if each of the five E_g modes of scheelite splits into one A_g plus one B_g mode, the 18 modes of fergusonite are obtained. On the other hand, the structural changes that occur at the phase transition[12−14] are expected to induce larger changes in the frequencies of the external modes as observed (see the low-frequency region in Figures 1 and 2). An interesting fact to highlight is that the most intense Raman modes of scheelite "are transformed" into the strongest modes in the fergusonite phase. This observation is consistent with the behavior observed at the analogous transition in related tungstates[35] and molybdates.[17] Another fact that points to the structural similarity between scheelite and fergusonite is the presence of a phonon gap between 400/500 and 800 cm^{-1} in both structures.

According to the present experiment, fergusonite $CaWO_4$ is the only phase detected from 11 to 31.6 GPa. In this pressure range, the Raman spectrum gradually evolves (see Figure 1) and no other phonons than the 18 modes of fergusonite are detected. Above 31.6 GPa additional changes occur. This is shown in Figure 3, where Raman spectra measured from 34.4 to 46.3 GPa are displayed. There, changes occurring at 34.4 GPa can be seen. In particular, at least 12 new Raman modes (denoted by * in the figure) appear at 34.4 GPa. They can be related to the onset of a second HP phase transition. Upon further compression, the Raman modes of fergusonite gradually vanish and the new modes become more prominent. The last traces of fergusonite can be seen at 39.4 GPa. In particular, the most intense mode of fergusonite (the highest frequency one) can still be detected at this pressure. At 43.3 GPa all the modes of fergusonite have disappeared, and therefore we assume the transition to the second HP phase is completed. At 46.3 GPa we detect a total of 15 bands that can be associated with Raman phonons of the new HP phase of $CaWO_4$. Their frequencies are 139, 184, 225, 337, 384, 404, 488, 609, 653, 729, 774, 795, 884, 984, and 1000 cm^{-1}. We give these values to facilitate comparison with them in future studies.

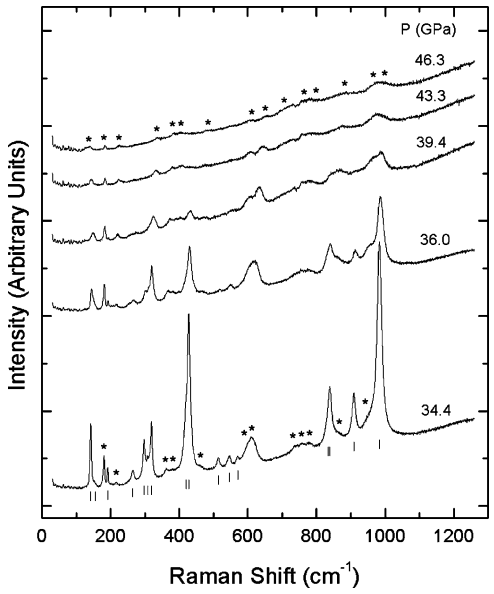

Figure 3. Selection of Raman spectra collected under compression from 34.4 to 46.3 GPa. The asterisks show the 12 peaks appearing at 34.4 GPa, indicating the onset of a second phase transition and the 15 bands identified for the new HP phase at 46.3 GPa. Ticks identify the fergusonite Raman modes at 34.4 GPa.

The most distinctive features of the Raman spectra of the new HP phase are (1) Raman modes are much broader and weaker than in scheelite and fergusonite; (2) the highest frequency mode detected is at a lower frequency than in fergusonite; (3) there are Raman modes appearing within the frequency region corresponding to the phonon gap of scheelite and fergusonite (see the 600−800 cm^{-1} region in Figure 4); and (4) there is an increase in the number of Raman modes in the high-frequency region. Unfortunately, the new HP phase is found as a pure phase only at two different pressures, 43.3 and 46.3

dx.doi.org/10.1021/ic5012555 | Inorg. Chem. 2014, 53, 9729−9738

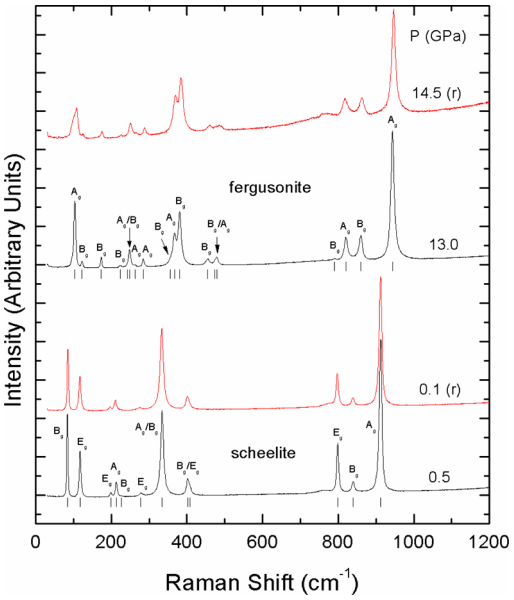

Figure 4. Selection of Raman spectra collected under compression (black) and decompression (red). The two spectra on the top correspond to the fergusonite phase, and the two spectra on the bottom to the scheelite phase. (r) is used to indicate the decompression pressure. Ticks are given to identify Raman modes together with the mode assignment.

GPa. Therefore, we will limit the discussion to mention its possible existence, leaving the assignation of its possible structure to the next section, where we discuss our calculations in detail. We would like to just mention here that, according to *ab initio* calculations, the post-fergusonite phase of $CaWO_4$ is predicted to have an orthorhombic structure, which doubles the formula unit per unit cell of the other two phases and belongs to space group *Cmca*. We would like to note here also that a similar structure has been proposed to be the post-fergusonite phase in $TbVO_4$.[15] The changes observed at this transition in the Raman spectrum of $TbVO_4$ are similar to those observed here at the second transition. If the orthorhombic *Cmca* structure is the new HP phase of $CaWO_4$, then it would involve a coordination increase for W from tetrahedral to octahedral and an increase of the W−O distances.[15] An obvious consequence would be the increase in the number of internal modes due to the change of coordination of W. Another possible consequence of this would be a decrease of the bond strength, which will cause a frequency drop in the internal stretching modes[40] (those at the highest frequencies), as observed in our experiments. Obviously from Raman spectroscopy alone it is not possible to identify the actual structure of the new HP phase of $CaWO_4$. Thus, new HP XRD studies are needed to accurately identify the crystal structure of the post-fergusonite phase of $CaWO_4$.

Before concluding this section, we would like to mention that, on pressure release, all detected transitions were reversible with little hysteresis. This fact is illustrated in Figure 4 by the Raman spectra collected on decompression at 14.5 and 0.1 GPa. In particular, the fergusonite phase was recovered as a pure phase at 26.2 GPa, and scheelite was fully recovered at 8.5 GPa. We would like to add here a comment on a possible pressure-driven amorphization[41] or chemical decomposition,[42] which was previously reported in $CaWO_4$ and related oxides. No evidence of chemical decomposition was found in our experiments. In particular, the reversibility of the changes observed in the Raman spectra supports that it does not occur up to 46.3 GPa. On the other hand, the presence of broad but well-defined Raman peaks up to the highest pressure covered by experiments implies that total amorphization of $CaWO_4$ does not occur. However, the intensity loss observed after the second phase transition might mean that the creation of amorphous clusters cannot be disregarded. In fact, a frustrated phase transition to the proposed orthorhombic structure with some amorphous component might be compatible with a reversible phase transition where the crystalline clusters might act as recrystallization seeds, reverting back to the transformation under pressure release. This hypothesis should be clarified by future studies, in particular by the extension of previous HP X-ray absorption experiments to higher pressure. The use of a quasi-hydrostatic medium in these experiments is crucial since it has been shown in related compounds that amorphization and decomposition could be caused by deviatoric stresses.[43]

To conclude with the description of the experiments, we would like to comment that color changes were observed in the $CaWO_4$ crystal under compression. In the scheelite phase $CaWO_4$ is colorless and transparent at all pressures. After the scheelite-to-fergusonite transitions no color change is detected up to 34.4 GPa. At this pressure the sample becomes yellowish. Additionally, macroscopic defects can be visually detected in the sample. After the second transition is completed, at 43.3 GPa, $CaWO_4$ becomes reddish. The first color change is consistent with the gradual band gap closing induced by pressure in fergusonite $CaWO_4$.[36] Indeed, the extrapolation of the results previously reported[36] gives at 34.4 GPa an optical band gap of 2.4 eV for fergusonite $CaWO_4$, which is consistent with the yellowish color of our sample at this pressure. The second color change suggests that the new HP phase of $CaWO_4$ has a smaller band gap than the other two phases. This fact should have consequences in the electrical transport properties of $CaWO_4$, which could be confirmed by HP electrical measurements like those already performed in $BaWO_4$.[44] As we will discuss below, *ab initio* calculations support these conclusions.

5. CALCULATIONS

We compare now our experiments with our theoretical study. Along with the observed scheelite and fergusonite phases, we have also considered previously proposed HP phases of related compounds[6] such as the orthorhombic structure (SG *Cmca*, 64, $Z = 8$) we previously predicted to exist in $CaWO_4$ beyond 29 GPa.[13] As mentioned above, the present calculations have been carried using two different GGA functionals for the exchange−correlation term, PBE and PBESOL, and also with CA LDA functionals. GGA calculations give an accurate description of the scheelite structure at ambient pressure. In contrast, LDA calculations underestimate the unit-cell volume and overestimate the bulk modulus. Figure 5 shows the energy−volume and enthalpy−pressure curves for the structures of $CaWO_4$ that we found to be stable under compression (for PBE). This figure shows the scheelite phase as being stable at zero and low pressure. Its compression is well described by a third-order Birch−Murnaghan equation of state (EOS), with V_0 = 325.64 (308.49) Å^3, B_0 = 73 (80.94) GPa, and B_0' = 4.48 (4.38) for PBE (PBESOL) calculations. These values compare well with the experimental results,[13] taking into account typical differences between DFT calculations and experiments, indicating that our GGA calculations reproduce well the HP behavior of scheelite $CaWO_4$. LDA calculations give the following EOS V_0 = 291.91 Å^3, B_0 = 93.94 GPa, and B_0' = 4.71. The comparison of the different EOS parameters clearly shows that GGA calculations describe better than LDA calculations the pressure behavior of scheelite-type $CaWO_4$. GGA PBE gives also transition pressures that agree better than LDA calculations with the experiments. Therefore, for the rest of the results presented here we will concentrate on GGA PBE/PBESOL calculations. Before discussing the theoretical results on pressure-driven transitions we would like to mention that the fact that GGA works better than LDA in scheelite $CaWO_4$ does not mean that the same will happen with other scheelite-

dx.doi.org/10.1021/ic5012555 | Inorg. Chem. 2014, 53, 9729−9738

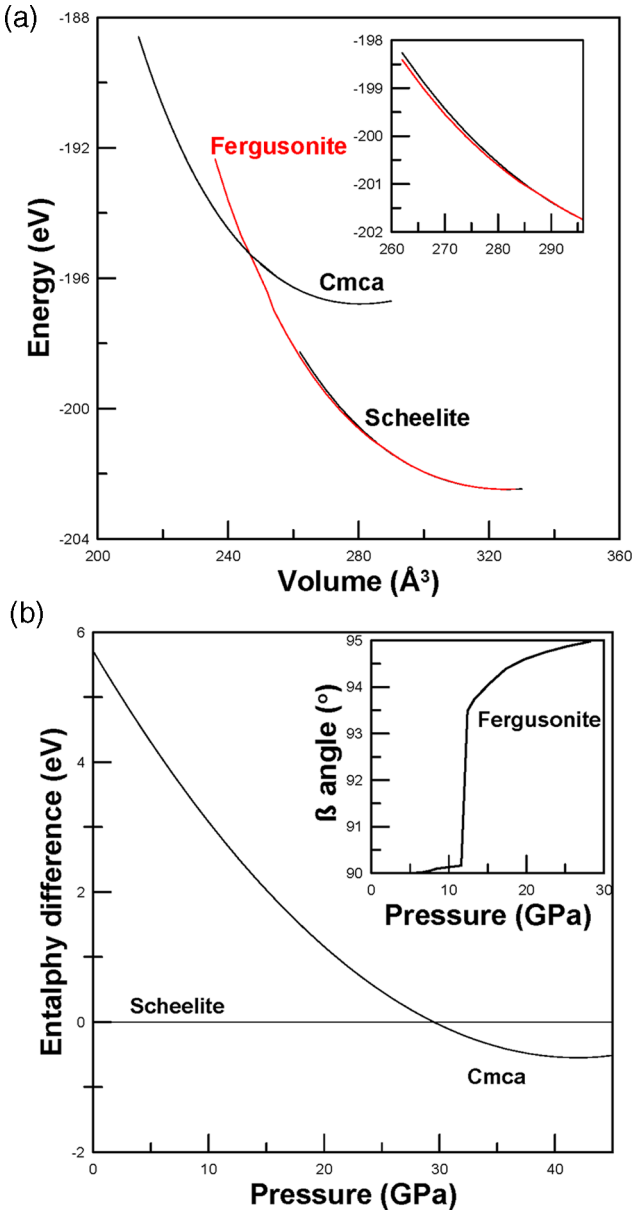

Figure 5. (a) Total-energy vs unit-cell volume (normalized to volume of scheelite). The inset is given to illustrate the small energy difference between scheelite (black) and fergusonite (red). (b) Differences in enthalpy vs pressure with respect to the scheelite phase. The inset shows the pressure evolution of the β angle of the fergusonite structure.

structure oxides. For example in germanates LDA works better than GGA.[45,46]

As pressure increases, the scheelite structure becomes unstable against fergusonite, which emerges as a stable phase above 10.7 GPa for PBE (9 GPa for PBESOL), in agreement with present and previous experiments.[11−14] The scheelite-to-fergusonite transition is very subtle, and enthalpy differences are too small to be distinguished in a plot (indeed the enthalpies of scheelite and fergusonite are indistinguishable in Figure 5b). Total-energy differences between both structures are also small (see Figure 5a). In particular, structural optimization indicates that the fergusonite structure, which is a slight monoclinic distortion of the scheelite structure, reduces to scheelite below the transition pressure. This can be seen in the inset of Figure 5b, where we represent the monoclinic β angle of the fergusonite phase versus pressure, a parameter that clearly illustrates the occurrence of the scheelite−fergusonite transition. The β angle becomes different from 90° only above the transition pressure. At the same pressure also the degeneracy of the tetragonal a-axis of scheelite is broken. Upon further compression we found that a structure with orthorhombic symmetry (SG no. 64, *Cmca*) has a lower enthalpy and energy than the other phases considered. The phase transition takes place above 21 GPa according to PBESOL calculations and at 29.4 GPa according to PBE calculations (see Figure 5). The second value agrees better with the experimental transition pressure. Structural details of the new orthorhombic structure are given in Table 3.

Table 3. Calculated Structural Parameters for the Orthorhombic Structure (SG *Cmca*) of $CaWO_4$

atom	site	x	y	z
P = 29.4 GPa, a = 7.398 Å, b = 12.267 Å, c = 5.068 Å				
Ca	8e	0.25	0.335 81	0.25
W	8f	0.0	−0.090 19	0.725 50
O	8e	0.25	0.150 51	0.25
O	8f	0.0	0.710 59	0.007 88
O	8d	0.34403	0.0	0.0
O	8f	0.0	0.584 80	0.591 30
P = 43.6 GPa, a = 7.303 Å, b = 11.913 Å, c = 5.000 Å				
Ca	8e	0.25	0.336 44	0.25
W	8f	0	−0.091 29	0.730 17
O	8e	0.25	0.151 51	0.25
O	8f	0.0	0.714 98	0.004 11
O	8d	0.34249	0.0	0.0
O	8f	0.0	0.582 27	0.601 66

For the scheelite, fergusonite, and orthorhombic structures we have calculated the Raman-active modes. The frequency and pressure coefficients of the Raman modes are summarized in Tables 1, 2, and 4. For scheelite, the agreement between

Table 4. Calculated Raman Phonons for the Orthorhombic Structure at 43.6 GPa and Pressure Coefficients

Raman mode symmetry	ω_0 [cm^{-1}]	$d\omega/dP$ [cm^{-1}/GPa]	Raman mode symmetry	ω_0 [cm^{-1}]	$d\omega/dP$ [cm^{-1}/GPa]
B_{1g}	96.9	0.40	B_{3g}	448.3	0.11
B_{3g}	136.1	2.1	B_{1g}	451.1	2.40
B_{1g}	142.7	1.80	B_{1g}	482.8	1.74
A_g	164.4	1.41	A_g	514.4	1.49
B_{1g}	207.7	0.40	B_{2g}	530.4	0.86
B_{3g}	222.1	1.50	B_{3g}	576.5	1.64
A_g	229.0	0.66	A_g	591.6	3.50
B_{2g}	238.9	0.47	B_{3g}	594.7	0.99
B_{2g}	279.3	1.20	B_{2g}	602.8	1.74
B_{3g}	297.5	1.20	B_{1g}	715.6	3.10
B_{1g}	302.7	0.86	A_g	725.1	1.16
A_g	315.1	1.82	B_{3g}	728.8	0.94
B_{2g}	333.9	1.70	A_g	745.8	0.28
B_{3g}	335.8	0.59	B_{2g}	785.7	2.99
B_{1g}	337.9	3.77	B_{1g}	789.8	2.63
B_{2g}	381.9	1.51	B_{3g}	791.0	2.98
B_{3g}	385.5	−0.13	A_g	811.5	1.94
A_g	396.6	1.68	B_{3g}	900.6	2.15

dx.doi.org/10.1021/ic5012555 | *Inorg. Chem.* 2014, 53, 9729−9738

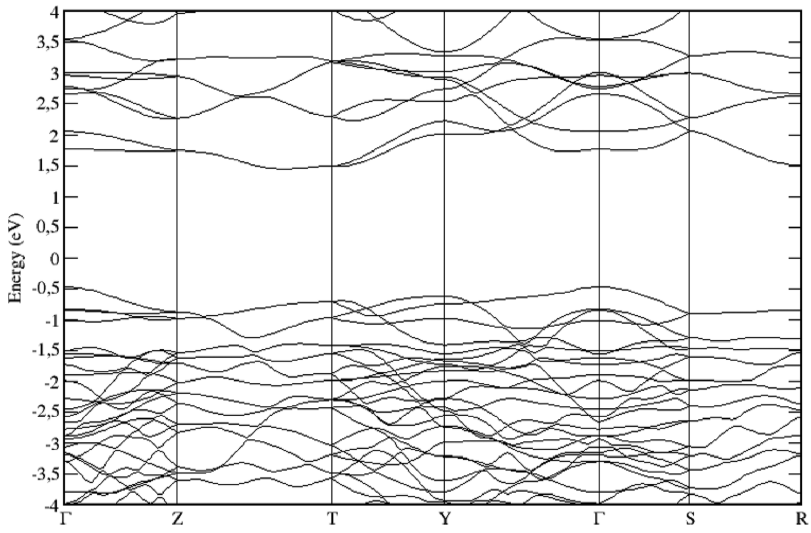

Figure 6. Calculated band structure of the orthorhombic structure of $CaWO_4$ at 35 GPa along the high-symmetry directions.

calculations and experiments is quite good (see Table 1). In particular, the coincidence is better with the present quasi-hydrostatic experiment than with previous experiments carried out under less hydrostatic conditions. Phonon frequencies are all slightly underestimated by calculations. For PBESOL calculations the phonon frequencies agree within 4% with our experiments, with the exception of the lowest frequency B_g mode, whose measured frequency is 85 cm^{-1} and the calculated one is 76 cm^{-1}. For PBE calculations the phonon frequencies agree within 6% with experiments, larger differences being observed only for the rotational modes (see Table 1). Interestingly, according to PBESOL, the $\upsilon_2(A_g)$ and $\upsilon_2(B_g)$ follow the same order as determined from experiments. However, PBE gives an inverse order (see Table 1), but frequency differences of these "nearly degenerate" modes are comparable with experimental and computational accuracy. Regarding pressure coefficients, only those of the lowest B_g frequency mode and the $R(A_g)$ mode are significantly overestimated. However, both calculations and experiments found the B_g mode to be a soft mode. For fergusonite the agreement between calculations and present experiments is also good. In particular, differences in frequencies are less than 10%. Again, as for scheelite, PBESOL and PBE give a different order for two modes, the "nearly degenerate" A_g and B_g modes of fergusonite with frequencies near 340 cm^{-1}. Differences in pressure coefficients are a bit larger, but the overall description of the pressure behavior of different modes is reasonable. Calculations also give a nonlinear behavior for some of the modes found to have nonlinear pressure dependences in experiments. Before discussing the Raman modes of the new orthorhombic structure, we would like to comment that all our phonon calculations have been carried out within the harmonic approximation. The good comparison of calculations with experiments suggests that anharmonicity does not play an important role in the room-temperature HP behavior of the Raman-active modes of $CaWO_4$. A deeper discussion on the effect of anharmonicity is beyond the scope of this work.

The Raman modes calculated for the orthorhombic structure are shown in Table 4. This structure has 36 Raman-active modes: Γ = 9 A_g + 9 B_{1g} + 7 B_{2g} + 11 B_{3g}. Note that many modes have close frequencies, which could explain the detection of broad bands in the experiments. The calculated pressure coefficients are summarized in Table 4. A quantitative comparison with experiments cannot be done because in the experiments only broad bands are detected (see Figure 3). However, with the exception of the broad band observed in experiments near 1000 cm^{-1}, the other bands observed in the second HP phase have frequencies similar to frequencies calculated for the orthorhombic structure. A remarkable feature of the orthorhombic structure is that, according to calculations, the phonon gap present in scheelite and fergusonite disappears in the orthorhombic structure. Another interesting fact of the orthorhombic structure is the presence of three soft modes, as can be seen in Table 4. Unfortunately, the existence of the orthorhombic *Cmca* structure cannot be confirmed with Raman experiments only. Thus, our results are calling for new HP X-ray diffraction experiments in $CaWO_4$ beyond 28 GPa searching for the orthorhombic structure proposed here. It is interesting to note that evidence of such a structure has already been reported as a post-scheelite phase in $TbVO_4$ and $SrMoO_4$.[15−17] This structure has also been theoretically predicted for $SrWO_4$.[13] However, a different phase with monoclinic structure was found in $BaWO_4$ and $PbWO_4$.[16,47] Clearly the reached HP polymorphism of orthotungstates deserves to be further studied.

The electronic band structure of the scheelite and fergusonite structures of $CaWO_4$ have already been studied extensively by us at ambient and high pressure.[21] As discussed above, these results fully agree with the present and previous findings. Therefore, we will concentrate our efforts on calculating only the electronic band structure of the new orthorhombic structure. The calculated band structure at 35 GPa (a pressure where the *Cmca* phase is predicted to be stable) is shown in Figure 6. There it can be seen that orthorhombic $CaWO_4$ is a semiconductor material with an indirect band gap. The top of the valence band is at the Γ point of the Brillouin zone, and the bottom of the conduction band at the R point. The calculated band gap at 35 GPa is 2 eV (in fergusonite at 35 GPa it is 2.4 eV). This value implies a band gap collapse of around 0.4 eV at the fergusonite−*Cmca* transition. The band gap collapse is consistent with the color change we observed for $CaWO_4$ in the experiments near 35 GPa. According to our calculations, the band gap of the orthorhombic structure gradually closes under compression at −20 meV/GPa; therefore if no further phase

dx.doi.org/10.1021/ic5012555 | *Inorg. Chem.* 2014, 53, 9729−9738

transition occurs, an extrapolation of our results suggests that $CaWO_4$ will not metalize up to 135 GPa.

6. CONCLUDING REMARKS

Raman experiments have been carried out under quasi-hydrostatic conditions in $CaWO_4$ up to 46.3 GPa, extending the pressure range covered by previous nonhydrostatic experiments by more than 20 GPa. *Ab initio* calculations have been carried out for the same compound. Our study confirms that the low-pressure scheelite phase undergoes a reversible scheelite-to-fergusonite phase transition above 9.7 GPa. Evidence of a second reversible (and previously unknown) transition is found in the experiments at 34.4 GPa. This transition is completed only at 43.3 GPa. No further change in the Raman spectrum is detected up to 46.6 GPa. The pressure evolution of the 13 (18) Raman modes of scheelite (fergusonite) $CaWO_4$ is also reported. For the HP fergusonite phase this is the first time that all its modes and their pressure dependences are measured. In this phase a nonlinear behavior is observed in several modes. The theoretical description of Raman modes of the scheelite and fergusonite phases is in good agreement with experiments. In particular, calculations helped to deconvolute Raman modes of fergusonite that are very close in frequency and that previously were assigned to only one mode. Regarding the new HP phase, the frequencies of the 15 modes detected in the experiments are also given. Calculations identify the new HP phase as an orthorhombic structure belonging to space group *Cmca*. Details of this structure are reported as well as its 36 Raman-active modes and their pressure coefficients. Furthermore, the electronic band structure of the new orthorhombic phase of $CaWO_4$ is studied in detail by means of *ab initio* calculations. These results explain the color change observed in the sample near 35 GPa. Results are compared with those reported in previous experiments performed under nonhydrostatic conditions. As observed in related oxides,[48] the new HP phase of $CaWO_4$ has apparently a smaller band gap than the already known phases. One remarkable property of this compound is that the original scheelite structure is recovered from the highest pressure reached in the experiment, through two phase transitions. The results reported here call for new XRD experiments to accurately determine the crystal structure of the new HP phase of $CaWO_4$.

AUTHOR INFORMATION

Corresponding Author

*E-mail: daniel.errandonea@uv.es.

Author Contributions

The manuscript was written through contributions of all authors. All authors have given approval to the final version of the manuscript.

Notes

The authors declare no competing financial interest.

ACKNOWLEDGMENTS

Research was supported by the Spanish government MINECO under grant nos. MAT2010-21270-C04-01/03, MAT2013-46649-C4-1/3, and CSD2007-00045. We also acknowledge the computer time provided by MALTA cluster and the Red Española de Supercomputación (RES).

REFERENCES

(1) Sleight, A. W. *Acta Crystallogr. B* **1972**, *28*, 2899−2902.
(2) Ninković, J.; Angloher, G.; Bucci, C.; Cozzini, C.; Frank, T.; Hauff, D.; Kraus, H.; Majorovits, B.; Mikhailik, V.; Petricca, F.; Pröbst, F.; Ramachers, Y.; Rau, W.; Seidel, W.; Uchaikin, S. *Nucl. Instrum. Methods Phys. Res. A* **2005**, *537*, 339−343.
(3) Faure, N.; Borel, C.; Couchaud, M.; Basset, G.; Templier, R.; Wyon, R. C. *Appl. Phys. B: Laser Opt.* **1996**, *63*, 593−598.
(4) Mahlik, S.; Behrendt, M.; Grinberg, M.; Cavalli, E.; Bettinelli, M. *Opt. Mater.* **2012**, *34*, 2012−2016.
(5) Brenier, A.; Jia, G.; Tu, C. *J. Phys.: Condens. Matter* **2004**, *16*, 9103−9108.
(6) Errandonea, D.; Manjon, F. J. *Prog. Mater. Sci.* **2008**, *53*, 711−773.
(7) Goncharov, A. F. *Int. J. Spectrosc.* **2012**, *2012*, 617528.
(8) Porto, S. P. S.; Scott, J. F. *Phys. Rev.* **1967**, *157*, 716−719.
(9) Nicol, M.; Durana, J. F. *J. Chem. Phys.* **1971**, *54*, 1436−1441.
(10) Jayaraman, A.; Batlogg, B.; Van Uitert, L. G. *Phys. Rev. B* **1983**, *28*, 4774−4778.
(11) Christofilos, D.; Ves, S.; Kourouklis, G. A. *Phys. Status Solidi B* **1996**, *198*, 539−544.
(12) Grzechnik, A.; Crichton, W. A.; Hanfland, M.; Van Smaalen, S. *J. Phys.: Condens. Matter* **2003**, *15*, 7261−7270.
(13) Errandonea, D.; Pellicer-Porres, J.; Manjon, F. J.; Segura, A.; Ferrer-Roca, Ch.; Kumar, R. S.; Tschauner, O.; Rodríguez-Hernández, P.; López-Solano, J.; Radescu, S.; Mujica, A.; Muñoz, A.; Aquilanti, G. *Phys. Rev. B* **2005**, *72*, 174106.
(14) Vilaplana, R.; Lacomba-Perales, R.; Gomis, O.; Errandonea, D.; Meng, Y. *Solid State Sci.* **2014**, *36*, 16−23.
(15) Errandonea, D.; Manjón, F. J.; Muñoz, A.; Rodríguez-Hernández, P.; Panchal, V.; Achary, S. N.; Tyagi, A. K. *J. Alloys Compd.* **2013**, *577*, 327−335.
(16) Gomis, O.; Sans, J. A.; Lacomba-Perales, R.; Errandonea, D.; Meng, Y.; Chervin, J. C.; Polian, A. *Phys. Rev. B* **2012**, *86*, 054121.
(17) Errandonea, D.; Gracia, L.; Lacomba-Perales, R.; Polian, A.; Chervin, J. C. *J. Appl. Phys.* **2013**, *113*, 123510.
(18) Nikl, M.; Bohacek, P.; Mihokova, N.; Kobayashi, M.; Ishii, M.; Usuki, Y.; Babin, V.; Stolovich, A.; Zazubovich, S.; Bacci, M. *J. Lumin.* **2000**, *87*−*89*, 1136−1139.
(19) Klotz, S.; Chervin, J. C.; Munsch, P.; Le Marchand, G. *J. Phys. D: Appl. Phys.* **2009**, *42*, 075413.
(20) Mao, H. K.; Xu, J.; Bell, P. M. *J. Geophys. Res.* **1986**, *91*, 4673−4676.
(21) Lacomba-Perales, R.; Errandonea, D.; Segura, A.; Ruiz-Fuertes, J.; Rodriguez-Hernandez, P.; Radescu, S.; Lopez-Solano, S.; Mujica, A.; Muñoz, A. *J. Appl. Phys.* **2011**, *110*, 043703.
(22) Hohenberg, P.; Kohn, W. *Phys. Rev.* **1964**, *136*, B864−B871.
(23) Kresse, G.; Furthmüller, J. *Phys. Rev. B* **1996**, *54*, 11169−11186. Kresse, G.; Joubert, D. *Phys. Rev. B* **1999**, *59*, 1758−1775.
(24) Blöchl, P. E. *Phys. Rev. B* **1994**, *50*, 17953−17978. Hafner. *J. Comput. Chem.* **2008**, *29*, 2044−2078.
(25) Perdew, J. P.; Burke, K.; Ernzerhof, M. *Phys. Rev. Lett.* **1996**, *77*, 3865−3868.
(26) Perdew, J. P.; Ruzsinszky, A.; Csonka, G. I.; Vydrow, O. A.; Scuseria, G. E.; Constantin, L. A.; Zhou, X.; Burke, K. *Phys. Rev. Lett.* **2008**, *100*, 136406.
(27) Ceperley, D. M.; Alder, B. J. *Phys. Rev. Lett.* **1980**, *45*, 566−569.
(28) Perdew, J. P.; Zunger, A. *Phys. Rev. B* **1981**, *23*, 5048−5079.
(29) Monkhorst, H. J.; Pack, J. D. *Phys. Rev. B* **1976**, *13*, 5188−5192.
(30) Mujica, A.; Rubio, A.; Muñoz, A.; Needs, R. J. *Rev. Mod. Phys.* **2003**, *75*, 863−912.
(31) Parlinsky, K. Computer Code PHONON; http://wolf.ifj.edu.pl/phonon.
(32) Panchal, V.; Errandonea, D.; Segura, A.; Rodriguez-Hernandez, P.; Muñoz, A.; Lopez-Moreno, S.; Bettinelli, M. *J. Appl. Phys.* **2011**, *110*, 043723.
(33) Ruiz-Fuertes, J.; Lopez-Moreno, S.; Errandonea, D.; Segura, A.; Lacomba-Perales, R.; Muñoz, A.; Radescu, S.; Rodriguez-Hernandez, P.; Gospodinov, L.; Tu, C. Y. *Phys. Rev. B* **2012**, *86*, 125202.

(34) Yu, P.; Cardona, M. *Fundamentals of Semiconductors*, 2nd ed.; Springer-Verlag: Berlin, 2003.
(35) Manjón, F. J.; Errandonea, D.; Garro, N.; Pellicer-Porres, J.; Rodríguez-Hernández, P.; Radescu, S.; López-Solano, J.; Mujica, A.; Muñoz, A. *Phys. Rev. B* **2006**, *74*, 144111.
(36) Russell, J. P.; Loudon, R. *Proc. Phys. Soc.* **1965**, *85*, 1029−1033.
(37) Errandonea, D.; Manjon, F. J. *Mater. Res. Bull.* **2009**, *44*, 807−811.
(38) Liarokapis, E.; Calamiotou, M.; Zhigadlo, N. D.; Katrych, S.; Karpinski, J. *J. Phys. Chem. Solids* **2013**, *74*, 1465−1469.
(39) Errandonea, D. *EPL* **2007**, *77*, 56001.
(40) Hofmeister, A. M. *Phys. Rev. B* **1997**, *56*, 5835−5855.
(41) Errandonea, D.; Somayazulu, M.; Häusermann, D. *Phys. Status Solidi B* **2003**, *235*, 162−169.
(42) Grzechnik, A.; Crichton, W. A.; Hanfland, M. *Phys. Status Solidi B* **2005**, *242*, 2795−2802.
(43) Ruiz-Fuertes, J.; Errandonea, D.; Gomis, O.; Friedrich, A.; Manjón, F. J. *J. Appl. Phys.* **2014**, *115*, 043510.
(44) Li, Y.; Gao, Y.; Han, Y.; Liu, C.; Ren, W.; Wang, Q.; Ma, Z.; Wu, B.; Gao, Ch. *J. Phys. Chem. C* **2012**, *116*, 25198−25205.
(45) Shwetha, G.; Kanchana, V.; Ramesh Babu, K.; Vaitheeswaran, G.; Valsakumar, M. C. *J. Phys. Chem. C* **2014**, *118*, 4325−4333.
(46) Errandonea, D.; Kumar, R. S.; Gracia, L.; Beltran, A.; Achary, S. N.; Tyagi, A. K. *Phys. Rev. B* **2009**, *80*, 094101.
(47) Errandonea, D.; Pellicer-Porres, J.; Manjon, F. J.; Segura, A.; Ferrer-Roca, Ch.; Kumar, R. S.; Tschauner, O.; Rodríguez-Hernández, P.; López-Solano, J.; Radescu, S.; Mujica, A.; Muñoz, A.; Aquilanti, G. *Phys. Rev. B* **2006**, *73*, 224103.
(48) Errandonea, D.; Gomis, O.; García-Domene, B.; Pellicer-Porres, J.; Katari, V.; Achary, S. N.; Tyagi, A. K.; Popescu, C. *Inorg. Chem.* **2013**, *52*, 12790−12798.